Hydrogen-Bond Dynamics in a Protic Ionic Liquid: Evidence for Large-Angle Jumps

Johannes Hunger,[a,b] Thomas Sonnleitner,[c] Liyuan Liu,[a] Richard Buchner,[c] Mischa Bonn,[a,b] and Huib J. Bakker[a]
[a] *FOM Institute AMOLF, Science Park 104, 1098 XG Amsterdam, The Netherlands*
[b] *Max Planck Institute for Polymer Research, Ackermannweg 10, 55128 Mainz, Germany, hunger@mpip-mainz.mpg.de*
[c] *Institut für Physikalische und Theoretische Chemie, Universität Regensburg, Universitätsstraße 31, 93053 Regensburg, Germany*

SUPPORTING INFORMATION

I. SAMPLES

Ethylammonium nitrate (EAN) was purchased from Iolitec (purity > 99 %, Heilbronn, Germany). In the time-resolved infrared experiments part of the N-H groups were isotopically exchanged by adding a small amount of D_2O (99.9 %, Sigma-Aldrich).

We prepared samples at isotopic exchange ratios ranging from $x = 0.020$ to 0.286 ($C_2H_5ND_xH_{3-x}NO_3$). Due to fast isotopic exchange deuterium atoms are distributed statistically. Thus, singly substituted cations ($C_2H_5NH_2D^+$) are the dominant deuterated species in all samples. At high values of x $C_2H_5NHD_2^+$ ions are formed, which may complicate the vibrational structure of the molecules. However, at the highest isotopic exchange ratio ($x = 0.286$) the concentration of $[C_2H_5NHD_2]^+$ is ten times lower compared to the concentration of $[C_2H_5NH_2D]^+$ ions and is not contributing significantly to our experiments. At lower values of x $[C_2H_5NHD_2]^+$ molecules are even less significant.

The samples were subsequently dried at mild conditions (in vacuum over P_2O_5 at ambient temperature) to avoid evaporation of the volatile ethylamine and decomposition [1, 2]. The residual water content was determined to be < 0.5 % using linear infrared spectroscopy. The isotopic exchange ratio, x, for EAN was confirmed by measuring the infrared absorption at N-D stretching frequencies (Fig. S1).

We recorded linear infrared spectra, $\alpha(\omega)$, using a double beam mid-infrared spectrometer (Perkin-Elmer 881). The samples were contained between two CaF_2 windows separated by a Teflon spacer. We determined the densities of the samples, required for the calculation of molar concentrations (c in mol L^{-1}) from data reported in the literature [3].

We prepared the EAN sample for the dielectric spectroscopy experiment by reacting equimolar amounts of ethylamine with nitric acid. The water was removed by rotary evaporation followed by lyophilisation. The crude EAN was recrystallized thrice from acetonitrile and the resulting colorless liquid was dried for one week at < 10 mbar and 50 °C, and then stored under nitrogen atmosphere.

II. DIELECTRIC SPECTROSCOPY

A. Experiment

We measured complex permittivity spectra, $\hat{\eta}(\nu) = \eta'(\nu) - i\eta''(\nu)$ as a function of the frequency ν of an applied electric field, using a frequency-domain reflectometer (Agilent E8364B VNA combined with Agilent 85070E-020 (0.2-20 GHz) and 85070E-050 (0.5-50 GHz) probes and an ECal module. The raw VNA data were corrected for calibration errors with a Padé [4] approximation. At frequencies ranging from 27 to 89 GHz two variable path-length waveguide interferometers (IFMs) were used [5]. The temperature was controlled with an overall accuracy of ±0.05 °C at intervals of 10 °C over the range 5 °C –65 °C.

For electrically conducting samples of dc conductivity, κ, the generalized permittivity spectra, $\hat{\eta}(\nu)$ contains an additional Ohmic loss term, which originates from charge transport in the sample. The dielectric permittivity spectra, $\hat{\varepsilon}(\nu)$, are obtained by correcting for this effect:

$$\hat{\varepsilon}(\nu) = \hat{\eta}(\nu) + \frac{i\kappa}{2\pi\nu\varepsilon_0} \tag{1}$$

where ε_0 is the permittivity of free space. The conductivities κ of the EAN samples were determined using a three electrode sample cell that is temperature controlled within ±5 mK whose resistance was measured using a LCR-Bridge (HAMEG, HM8118) [6].

B. Data Analysis

Dielectric relaxation spectroscopy probes the macroscopic polarization of a sample. After conductivity correction (eq 1) the dielectric permittivity spectrum, $\hat{\varepsilon}(\nu) = \varepsilon'(\nu) - \mathrm{i}\varepsilon''(\nu)$ is obtained. In order to extract information on a molecular level, the spectrum is described with a sum of n individual functions with band-shape, $\tilde{F}_j$, and amplitude, S_j.

$$\hat{\varepsilon}(\nu) = \varepsilon_\infty + \sum_{j=1}^{n} S_j \cdot \tilde{F}_j(\nu) \tag{2}$$

$\varepsilon_\infty = \lim_{\nu\to\infty} \varepsilon'(\nu)$ is the permittivity at frequencies where only the intramolecular polarizability contributes to the polarization response.

The relaxation processes are described by the empirical Havriliak-Negami function (HN)

$$\tilde{F}_{j,\mathrm{HN}}(\nu) = \frac{1}{[1 + (\mathrm{i}2\pi\nu\tau_j)^{1-\alpha_j}]^{\beta_j}} \tag{3}$$

or its simplified variants, the Cole-Davidson (CD; $\alpha_j = 0$), Cole-Cole (CC; $\beta_j = 1$) and Debye equations (D; $\alpha_j = 0$, $\beta_j = 1$). In eq. 3 τ_j, is the relaxation time of mode j, whereas the parameters $0 \leq \alpha_j < 1$ and $0 < \beta_j \leq 1$ describe its symmetric and asymmetric broadening, respectively [7, 8]. These relaxation functions are unphysical at THz frequencies (and higher), since they assume that the sample reacts instantaneously to an applied electric field, which is impossible because of inertial effects. To correct for the inertial effect, Turton *et al.* [9] introduced an initial rise time, which in the frequency domain corresponds to a rise rate $\gamma_{\mathrm{lib}} \approx \langle\omega_{\mathrm{lib}}\rangle/2\pi = \langle\nu_{\mathrm{lib}}\rangle$ defined by the mean libration frequency.

For EAN we model the dominant relaxation process of the DR spectrum by an inertia-corrected Cole-Davidson function (CDi)

$$\tilde{F}_{\mathrm{CDi}}(\nu) = (S^0_{\mathrm{CDi}})^{-1} \cdot \left[\frac{1}{(1 + \mathrm{i}2\pi\nu\tau_{\mathrm{CDi}})^{\beta_{\mathrm{CDi}}}} - \frac{1}{(1 + \mathrm{i}2\pi\nu\tau_{\mathrm{CDi}} + \gamma_{\mathrm{lib}}\tau_{\mathrm{CDi}})^{\beta_{\mathrm{CDi}}}}\right] \tag{4}$$

with the normalization factor

$$S^0_{\mathrm{CDi}} = 1 - \frac{1}{(1 + \gamma_{\mathrm{lib}}\tau_{\mathrm{CDi}})^{\beta_{\mathrm{CDi}}}}. \tag{5}$$

Note that this function only represents the dominant low-frequency part of a more complex fit model that consists of several modes. This fit model is required to describe the dielectric spectra of EAN up to 10 THz [10]. We converted the correlation times, τ_{CDi}, obtained from the fit into relaxation times, $\tau_{\mathrm{DR}} = 1/2\pi\nu_{\mathrm{max}}$, that are associated with the frequency of the peak maximum, ν_{max}, according to Ref. [11],

$$\tau_{\mathrm{DR}} = \tau_{\mathrm{CDi}} \left[\tan\left(\frac{\pi}{2(\beta_{\mathrm{CDi}} + 1)}\right)\right]^{-1}. \tag{6}$$

III. FEMTOSECOND INFRARED EXPERIMENTS

A. Experiment

The femtosecond infrared experiments are based on a commercial Ti:sapphire regenerative amplifier system delivering 800 nm pulses at a repetition rate of 1 kHz. We generate mid-infrared pulses via a sequence of nonlinear optical conversion processes yielding pulses centered at a frequency of 2250 cm^{-1}, with a duration of $\sim$ 150 fs, a pulse energy of $\sim 5\,\mu$J, and a spectral width of $\sim$ 100 cm^{-1} (full width half maximum, FWHM) [12, 13]. We used the pulses in one-color pump-probe experiments by splitting the pulses into probe ($\sim 4\,\%$), reference ($\sim 4\,\%$), and pump pulses ($\sim 92\,\%$), using a CaF_2 wedged window.

We also performed two-color pump-probe experiments, in which the mid-infrared pump pulse can be tuned independently from the probe and reference pulses. The probe and reference pulses ($\sim 0.2\,\mu$J) are generated via difference-frequency generation between signal and idler pulses that are produced by an optical parametric amplifier [14]. The difference frequency mixing yields mid-infrared pulses with a duration of $\sim$ 50 fs and a spectral bandwidth

of $\sim 300\,\mathrm{cm}^{-1}$. The center frequency of these pulses was tuned between $2150\,\mathrm{cm}^{-1}$ to $2400\,\mathrm{cm}^{-1}$. The mid-infrared pump pulses are generated by frequency doubling of the idler that is generated in a separate parametric amplifier. The resulting doubled idler at 1 μm is mixed with a fresh part of the 800 nm pulse in a potassium niobate crystal to generate the difference frequency. The resulting pulses have a center wavelength of $2250\,\mathrm{cm}^{-1}$, an energy of $\sim 25\,\mu\mathrm{J}$, and a pulse duration of $\sim 50\,\mathrm{fs}$ ($\sim 100\,\mathrm{cm}^{-1}$ FWHM).

In both experiments the polarization of the pump pulse is set to an orientation of 45 ° with respect to the probe and the reference polarization, using a $\lambda/2$ plate. The time delay of the probe pulses with respect to the pump is varied with a variable path-length delay line. The three pulses are focused into the sample that is held between two CaF_2 windows. The pump and probe pulses are in spatial overlap, the reference is not in overlap with the pump and probe. The reference pulse is used to correct for pulse to pulse energy fluctuations in the probe beam [12].

The sample cell is mounted in a temperature controlled sample holder using a Peltier element. In the experiment we select alternatingly the parallel or perpendicular polarization component of the transmitted probe and reference beams (with respect to the pump) using a polarizer mounted on a rotation stage. Both the probe and the reference pulses are dispersed with a spectrograph on a liquid-nitrogen-cooled mercury-cadmium telluride detector. We measure the (pump-induced) transient absorption in the sample parallel ($\Delta\alpha_\parallel(\omega,t)$) and perpendicular ($\Delta\alpha_\perp(\omega,t)$) to the pump polarization as a function of delay time, t, and wavenumber, ω.

From the measured absorption changes $\Delta\alpha_\parallel(\omega,t)$ and $\Delta\alpha_\perp(\omega,t)$ the isotropic signal is constructed:

$$\Delta\alpha_{\mathrm{iso}}(\omega,t) = \frac{\Delta\alpha_\parallel(\omega,t) + 2\Delta\alpha_\perp(\omega,t)}{3} \tag{7}$$

The isotropic signal represents solely vibrational relaxation and is not affected by reorientation processes. Complementary to the isotropic signal the anisotropy parameter $R(t)$ can be constructed:

$$R(\omega,t) = \frac{\Delta\alpha_\parallel(\omega,t) - \Delta\alpha_\perp(\omega,t)}{3\Delta\alpha_{\mathrm{iso}}(\omega,t)}. \tag{8}$$

The parameter $R(t)$ is independent of vibrational relaxation and only represents the dynamics of the anisotropy of the excitation. These dynamics include the molecular reorientation of the excited molecules.

We note that for neat EAN ($x = 0$) a small induced absorption ($\Delta\alpha_{\mathrm{iso}} \approx 6 \cdot 10^{-4}$) is observed. This signal is instantaneously present after the pump-pulse excitation and does neither show any time dependence nor anisotropy. It very likely originates from the excitation of the overtone and/or combination vibrations [15] that are apparent as a background absorption for neat EAN (Fig. S1). We account for this contribution by subtracting this background from our transient data at $t > 0$. This correction is only significant for $R(t)$ at low isotopic exchange ratios $x \leq 0.035$.

B. Data Analysis

1. *Linear Infrared Spectra*

As can be seen in Fig. S1 an intense band at $\omega \approx 2300\,\mathrm{cm}^{-1}$ emerges with increasing x. It should be noted, that this band appears to be structured (Fig. S1). This structure partly originates from the background absorption of neat EAN and partly from the increased uncertainty in the spectra at $2350\,\mathrm{cm}^{-1}$ originating from atmospheric CO_2 absorption. After correcting for the background absorption of EAN the absorption band can be well described by a Gaussian band centered at $\omega = (2290 \pm 5)\,\mathrm{cm}^{-1}$. With increasing isotope exchange, x, the amplitude of this band increases linearly. This band can thus be assigned to the N-D stretching vibration [15].

2. *Isotropic Results*

As we indicate in the main text of the manuscript, the excited state relaxes rapidly (Figs. 2 and S2) to an intermediate energy level. Further relaxation leads to a successive population of lower energy levels, followed by a slow thermal equilibration process. We also show that fluctuations in the ND stretching frequency (spectral diffusion) do not contribute significantly to the isotropic vibrational dynamics.

We model the experimental isotropic data, $\Delta\alpha_{\mathrm{iso}}(\omega,t)$, using a four-state kinetic model (Fig. S3). In this model the excited state population decays with a characteristic time constant, τ_1. This relaxation leads to a transient population of an intermediate state 0^*. The intermediate state relaxes with a characteristic time τ_2 to lower energy levels ($0'$).

Further thermalization dynamics with an equilibration time τ_3 result in the fully equilibrated state $0''$. The relaxation is thus described with the following set of differential equations:

$$\begin{aligned} \mathrm{d}N(t)/\mathrm{d}t &= -N(t)/\tau_1 && (9)\\ \mathrm{d}N^*(t)/\mathrm{d}t &= +N(t)/\tau_1 - N^*(t)/\tau_2 && (10)\\ \mathrm{d}N'(t)/\mathrm{d}t &= +N^*(t)/\tau_2 - N'(t)/\tau_3 && (11)\\ \mathrm{d}N''(t)/\mathrm{d}t &= +N'(t)/\tau_3 && (12) \end{aligned}$$

where $N^j(t)$ corresponds to the time-dependent population of each state. In this model we assume only the excited state to be populated at $t = 0$ (i.e. $N(0) = 1$; $N^*(0) = N'(0) = N''(0) = 0$). The time-dependent isotropic signals are given by the sum of the transient spectra, σ^j, associated with each single state, j, multiplied by their time-dependent population:

$$\Delta\alpha_{\mathrm{iso}}(\omega, t) = N(t)\sigma(\omega) + N^*(t)\sigma^*(\omega) + N'(t)\sigma'(\omega) + N''(t)\sigma''(\omega) \quad (13)$$

The fits are shown in Figs. 2b and S2 and excellently describe the experimental isotropic data.

3. Anisotropy Results

From the isotropic results it follows that the vibrational excitation of the ND vibration is only present at early delay times, t, and that at later delays ($t > 5\,\mathrm{ps}$) the measured signals are dominated by thermal contributions (Fig. S4). The relaxation of the ND vibrations will at first lead to a local heating of the direct surroundings of the excited vibrations. These vibrations are preferentially aligned with the pump polarization. Hence, directly after the ND relaxation, the heating effect will be primarily felt by the originally excited oscillators, so that the thermal signal will retain the anisotropic character of the excitation. The anisotropy of the thermal signal can thus decay both as a result of the rotation of the originally excited ND group, and as a result of heat diffusion from the initially excited ND oscillators to not-excited, isotropically (randomly) oriented ND oscillators.

To quantify the contributions of the molecular rotation and the heat diffusion to the anisotropy decay, we describe the experimental data with a heat diffusion model. In this model we assume the excited ethylammonium ion and its neighboring ions to be a heated spherical particle of Radius P, at a temperature $T + \Delta T_{\mathrm{max}}$, and the surroundings to have a temperature T. The evolution of the temperature in the system as a function of time, t, and distance from the center of the sphere, r, can be expressed by [16]:

$$\Delta T(r,t) = \Delta T_{\mathrm{max}}\{\frac{1}{r}\sqrt{\frac{\chi}{\pi}t}\left[\exp\left(-\varepsilon_+^2\right) - \exp\left(-\varepsilon_-^2\right)\right] + \frac{1}{2}\left[\mathrm{erf}\left(\varepsilon_+\right) + \mathrm{erf}\left(\varepsilon_-\right)\right]\} \quad (14)$$

where $\varepsilon_\pm = (P \pm r)/(2\sqrt{\chi t})$, and erf is the Gaussian error function. χ represents the thermal diffusivity of the medium. The measured anisotropy of the thermal signal, $R_{\mathrm{h}}(t)$ can be related to the ratio between the energy in the excited particle and the average excess energy of all probe particles [16]:

$$R_{\mathrm{h}}(t) = \frac{\int_0^P r^2\Delta T(r,t)\mathrm{d}r}{\int_0^P r^2\Delta T(r,t)\mathrm{d}r + f\int_P^\infty r^2\Delta T(r,t)\mathrm{d}r} \quad (15)$$

where f is the volume fraction of probe molecules (i.e. ND oscillators whose absorption frequency coincides with the probe pulse bandwidth) in the sample. The value of $f = cxbN_{\mathrm{A}}P^3\pi 4/3$ is calculated from the experimental concentration, c, the isotope exchange ratio, x, and the probe particle volume, $P^3\pi 4/3$. N_{A} is the Avogadro constant. The factor b accounts for the narrow bandwidth of the infrared pump pulses (compared to the ND absorption band). Due to this difference in bandwidth only a subset of ND oscillators, whose absorption frequency coincide with the pump pulse bandwidth, is excited. The value of $b = 0.38$ is obtained from the overlap of the ND absorption band and the pump-pulse.

The thermal energy in the particle will not be present instantaneously (i.e. at $t = 0$), but evolves as the vibrational excitation decays and the energy dissipates to the local environment. We account for this delayed appearance of the thermal signal by convoluting $R_{\mathrm{h}}(t)$ with the time-dependent generation of the thermal state population, as obtained from the modeling of the isotropic data (see above):

$$R'_{\mathrm{h}}(t) = \int_{-\infty}^{\infty} R_{\mathrm{h}}(t-t')\frac{1}{\tau_2}N^*(t')\mathrm{d}t' \tag{16}$$

Further, we add the anisotropy of the vibrational excitations at early delay times :

$$R''_{\mathrm{h}}(t) = \phi_{\mathrm{ex}}(t) + (1-\phi_{\mathrm{ex}}(t))R'_{\mathrm{h}}(t) \tag{17}$$

The fraction $\phi_{\mathrm{ex}}(t) = (N(t)\sigma + N^*(t)\sigma^*)/\Delta\alpha_{\mathrm{iso}}(t)$ is given by the relative contribution of the vibrationally excited states (1, 0^*) to the overall isotropic signal, $\Delta\alpha_{\mathrm{iso}}(t)$, as inferred from the isotropic model. Finally, we include the contribution due to the rotation of the ND oscillators to the decay of the anisotropy:

$$R(t) = A_0 R''_{\mathrm{h}}(t)\mathrm{e}^{-t/\tau_{\mathrm{IR}}}, \tag{18}$$

with A_0 the anisotropy at $t = 0$ and the exponential term representing the decay of the anisotropy due to rotation, with a rotational correlation time τ_{IR}.

We model the experimental anisotropies at all isotopic exchange ratios, x, in a global fit, where χ, P, and τ_{IR} are the global fit parameters for each temperature. To allow for a lower initial value of the anisotropy (at $t = 0$) at higher concentrations of deuterium (e.g. due to rapid resonant energy transfer of the excitation at early delay times), the parameter A_0 is a free parameter at each concentration. The concentration, c, and the isotopic exchange ratio, x, are fixed to the experimental values. The results of the global fits of eq 18 to the experimental anisotropies are shown in Figs. 3 and S5. We estimate the uncertainty of the thus obtained parameters by fixing one parameter to a certain value while the other parameters remain free. The uncertainty corresponds to the range where the reduced error function does not increase by more than 5 %.

IV. SUPPLEMENTARY FIGURES

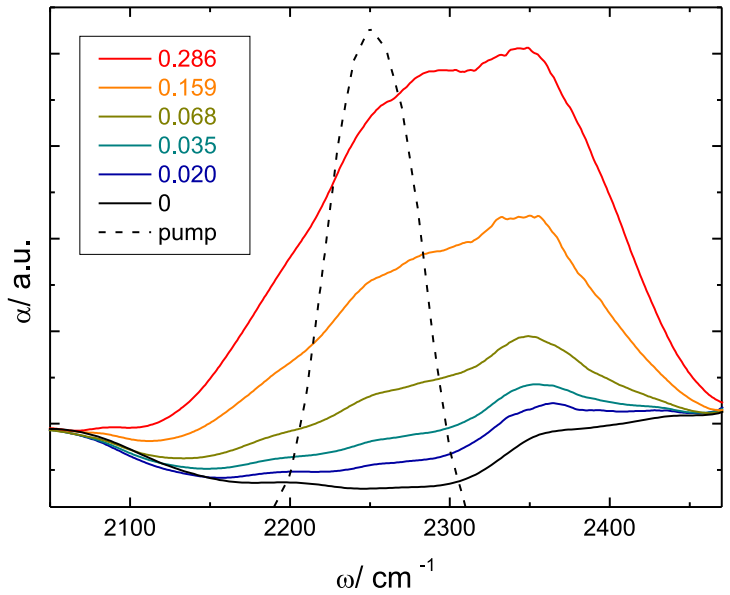

Figure S1: Infrared absorption spectra, $\alpha(\omega)$, of ethylammonium nitrate ($[C_2H_5NH_{3-x}D_x][NO_3]$) at ND stretching frequencies for different isotopic exchange ratios, x. Also shown is the background absorption of neat EAN ($x = 0$). The dotted black line corresponds to the spectrum of the pump pulse used in the femtosecond mid-infrared experiments.

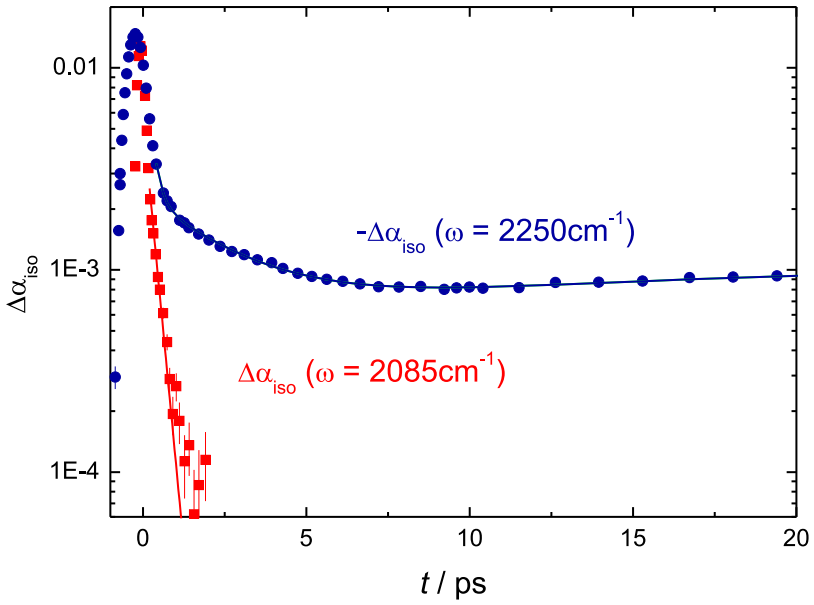

Figure S2: Isotropic transient absorption changes as a function of delay time for EAN with an isotopic exchange ratio of $x = 0.035$ at 25°C. The blue, filled circles show the negative isotropic signal $-\Delta\alpha_{\mathrm{iso}}(\omega = 2250\,\mathrm{cm}^{-1})$ where the bleaching due to the vibrational excitation dominates. The signal shows a very fast vibrational decay of the ND vibration at $t \leq 1\,\mathrm{ps}$, followed by a somewhat slower decay of the intermediate state ($1\,\mathrm{ps} \leq t \leq 6\,\mathrm{ps}$). At longer delay times ($t > 10\,\mathrm{ps}$) the effect of a slow thermalization process prevails. Also shown is the decay of the excited state absorption ($1 \rightarrow 2$ transition) $\Delta\alpha_{\mathrm{iso}}(\omega = 2085\,\mathrm{cm}^{-1})$ (red, filled squares). The rapid decay at these wavenumbers indicates that the vibrational excitation of the ND vibration is very short-lived. The lines represent the fit of the kinetic model described in section II.B.2 to the experimental data.

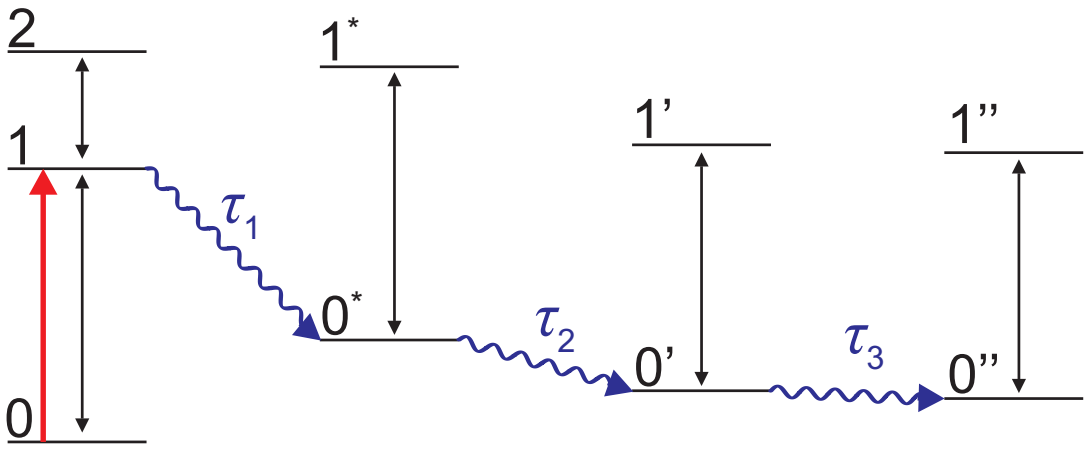

Figure S3: Schematic representation of the kinetic model used to describe the vibrational relaxation of $C_2H_5NH_2D^+$. An excited ND oscillator (1) decays with a time-constant τ_1 to an intermediate state, 0^*. The intermediate state consecutively relaxes with a time constant τ_2 to a heated state, $0'$. This state then equilibrates with a time constant τ_3 to a fully thermal final state $0''$. The transitions that contribute to the transient spectral response either as a result of depletion or generation of population in the different states are indicated by double arrows. The thick red arrow indicates the excitation of the N-D vibration by the pump pulse.

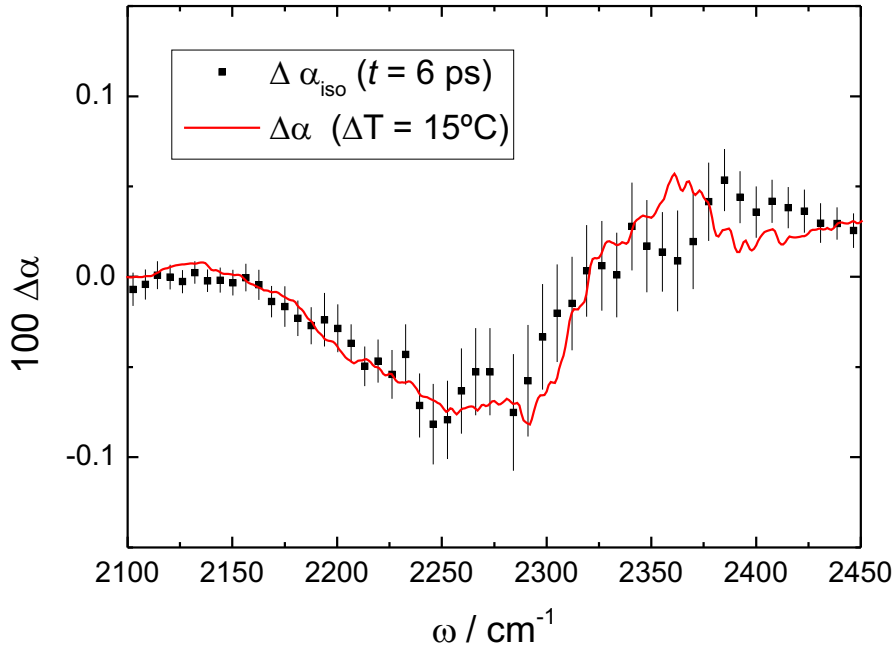

Figure S4: Isotropic transient absorption changes, $\Delta\alpha_{\mathrm{iso}}(\omega)$, for $x = 0.068$ at $t = 6\,\mathrm{ps}$ (symbols). Also shown is a thermal difference spectrum ($\Delta\alpha(\omega)$) for a temperature rise of $\Delta T = 15\,^{\circ}\mathrm{C}$ as obtained from linear infrared spectra measured at different temperatures. The agreement of the transient spectrum with the thermal difference spectrum shows that the heating of the sample prevails at these delays.

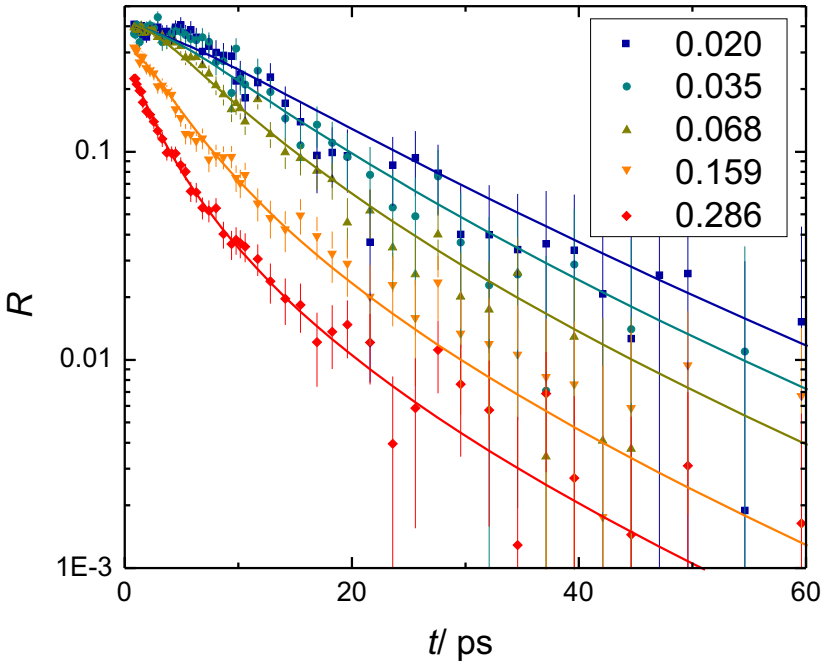

Figure S5: Anisotropy $R(t)$ of the transient absorption signal at 2250 cm^{-1} as a function of delay time for different isotopic exchange ratios, x, at 65 °C. The symbols show experimental data and the lines represent the results of the fits using eq 18.

[1] Krüger, M.; Bründermann, E.; Funkner, S.; Weingärtner, H.; Havenith, M. Polarity Fluctuations of the Protic Ionic Liquid Ethylammonium Nitrate in the Terahertz Regime. *J. Chem. Phys.* **2010,** *132,* 101101.

[2] Pinkert, A.; Ang, K. L.; Marsh, K. N.; Pang, S. Density, Viscosity and Electrical Conductivity of Protic Alkanolammonium Ionic Liquids. *Phys. Chem. Chem. Phys.* **2011,** *13,* 5136-5143.

[3] Allen, M.; Evans, D. F.; Lumry, R. Thermodynamic Properties of the Ethylammonium Nitrate + Water System: Partial Molar Volumes, Heat Capacities, and Expansivities. *J. Solution Chem.* **1985,** *14,* 549-560.

[4] Schrödle, S.; Hefter, G.; Kunz, W.; Buchner, R. Effects of the Non-Ionic Surfactant $C_{12}E_5$ on the Cooperative Dynamics of Water. *Langmuir* **2006,** *22,* 924-932.

[5] Barthel, J.; Buchner, R.; Eberspächer, P. N.; Münsterer, M.; Stauber, J.; Wurm, B. Dielectric Relaxation Spectroscopy of Electrolyte Solutions. Recent Developments and Prospects. *J. Mol. Liq.* **1998,** *78,* 83-109.

[6] Stoppa, A.; Hunger, J.; Buchner, R. Conductivities of Binary Mixtures of Ionic Liquids with Polar Solvents. *J. Chem. Eng. Data* **2009,** *54,* 472-479.

[7] Böttcher, C. F. J. *Theory of Electric Polarization;* volume 1 and 2 Elsevier: Amsterdam, 1978.

[8] Kremer, F.; Schönhals, A., Eds.; *Broadband Dielectric Spectroscopy;* Springer: Berlin, 2003.

[9] Turton, D. A.; Wynne, K. Structural Relaxation in the Hydrogen-Bonding Liquids *N*-Methylacetamide and Water Studied by Optical Kerr Effect Spectroscopy. *J. Chem. Phys.* **2008,** *128,* 154516.

[10] Turton, D. A.; Sonnleitner, T.; Ortner, A.; Walther, M.; Hefter, G.; Buchner, R.; Wynne, K. Structure and Dynamics in Protic Ionic Liquids: A Combined Ultrafast Optical Kerr Effect (OKE) & Dielectric Study. *Faraday Discuss.* **2012,** *154,* 145-153.

[11] Diaz-Calleja, R. Comment on the Maximum in the Loss Permittivity for the Havriliak-Negami Equation. *Macromolecules* **2000,** *33,* 8924.

[12] Bakker, H. J.; Rezus, Y. L. A.; Timmer, R. L. A. Molecular Reorientation of Liquid Water Studied with Femtosecond Mid-Infrared Spectroscopy. *J. Phys. Chem. A* **2008,** *112,* 11523-11534.

[13] Hunger, J.; Liu, L.; Tielrooij, K.-J.; Bonn, M.; Bakker, H. J. Vibrational and Orientational Dynamics of Water in Aqueous Hydroxide Solutions. *J. Chem. Phys.* **2011,** *135,* 124517.

[14] Hamm, P.; Kaindl, R. A.; Stenger, J. Noise Suppression in Femtosecond Mid-Infrared Light Sources. *Opt. Lett.* **2000,** *25,* 1789-1800.

[15] Zeroka, D.; Jensen, J. O.; Samuels, A. C. Infrared Spectra of Some Isotopomers of Ethylamine and the Ethylammonium Ion: A Theoretical Study. *J. Mol. Struct.: THEOCHEM* **1999,** *465,* 119-139.

[16] Liu, L.; Hunger, J.; Bakker, H. J. Energy Relaxation Dynamics of the Hydration Complex of Hydroxide. *J. Phys. Chem. A* **2011,** *115,* 14593-14598.